Journal of Catalysis **207,** 151–157 (2002)
doi:10.1006/jcat.2002.3539, available online at http://www.idealibrary.com on IDEAL®

The Preparation, Characterization, and their Photocatalytic Activities of Rare-Earth-Doped TiO_2 Nanoparticles

An-Wu Xu,[1] Yuan Gao, and Han-Qin Liu

Institute of Physical Chemistry, School of Chemistry and Chemical Engineering, Zhongshan University, Guangzhou 510275, China

Received July 24, 2000; revised March 26, 2001; accepted April 28, 2001

RE/TiO_2 photocatalysts were prepared by the sol–gel method using rare earth ($RE = La^{3+}$, Ce^{3+}, Er^{3+}, Pr^{3+}, Gd^{3+}, Nd^{3+}, Sm^{3+}) metal salts and tetra-*n*-butyl titanate as precursors, and were characterized by XRD, IR, UV–vis diffuse reflection, and transient absorption spectra. Their photocatalytic activities were evaluated using nitrite as a decomposition objective. As a result, suitable content of doping rare earth in TiO_2 can efficiently extend the light absorption properties to the visible region. At the same time, it is beneficial to NO_2^- adsorption over the catalysts due to rare earth doping. RE/TiO_2 samples can enhance the photocatalytic activity to some extent as compared with naked TiO_2. The increase in photoactivity is probably due to the higher adsorption, red shifts to a longer wavelength, and the increase in the interfacial electron transfer rate. Nitrite is almost completely degraded over RE/TiO_2 catalysts after longer irradiation, which is different from Degussa P-25 with a plateau of activity after ca. 20 min irradiation. Gd^{3+}-doped TiO_2 showed the highest reaction activity among all concerned RE-doped samples because of its specific characteristics. The amount of RE doping was an important factor affecting photocatalytic activity; the optimum amount of RE doping is ca. 0.5 wt%, at which each RE/TiO_2 sample shows the most reactivity. The photocatalytic degradation reaction of nitrite over Gd^{3+}-doped samples and P-25 follows apparent first order kinetics, which is different from that of Sm^{3+}, Ce^{3+}, Er^{3+}, Pr^{3+}, La^{3+}, and Nd^{3+}-doped TiO_2 catalysts, which obey zero-order kinetics, indicating that these processes were dominated by electron–hole recombination.

Key Words: **rare earth ions; TiO_2; sol–gel method; photocatalytic oxidation; nitrite.**

1. INTRODUCTION

Titania, as a photocatalyst, exhibits a number of attractive characteristics such as chemical stability, nontoxicity, low cost, and the highest oxidation rate of the many photoactive metal oxides investigated (1–7). Several reviews and books provide an overview of this research and an explanation of TiO_2-mediated photocatalytic process (1, 6). Although TiO_2 is the most widely used photocatalyst, its large bandgap ($E_g = 3.2$ eV) requires that near-UV light be used to photoactivate this very attractive photocatalyst. Unfortunately, in solar energy applications only ca. 3% of the solar light is absorbed. In recent years, attention has been paid to metal-doped titania specimens, testing their efficiency in replacing naked TiO_2 (8–17). So far, this technology has not been successfully commercialized, in part because of the low photocatalytic degradation efficiency on the surface of TiO_2 particles, which is due to the fast recombination rate of photogenerated electron–hole pairs. The quantum yields of most photocatalytic reactions are still extremely low and seldom exceed 1% in a liquid-phase photocatalytic system (18). In order to slow down the recombination rate of the electron–hole pairs and enhance interfacial charge-transfer efficiency, the properties of TiO_2 particles have been modified by selective surface treatments such as surface chelation, surface derivatization, platinization, and by selective metal ions doping TiO_2 (19–23).

There have been many reports on transition metal ion and noble metal dopants in TiO_2 investigated previously. The preparation of rare-earth-doped TiO_2 nanoparticles and their photocatalytic properties have seldom been reported so far.

In this paper, we present a comparative study on the photocatalytic efficiency of bare TiO_2 and rare-earth-doped titania prepared by the sol–gel method with precursors of rare earth nitrate salts and tetra-*n*-butyl titanate, and the enhanced photocatalytic performance of rare-earth-doped TiO_2 is demonstrated. RE/TiO_2 catalysts are also characterized by XRD, DRS, and transient absorption spectra.

2. EXPERIMENTAL

2.1. Catalyst Preparation

RE/TiO_2 particles were prepared by the sol–gel route using tetra-*n*-butyl titanate and the rare earth metal salts $La(NO_3)_3 \cdot 6H_2O$, $Ce(NO_3)_3 \cdot 6H_2O$, $Er(NO_3)_3 \cdot 5H_2O$, $Pr(NO_3)_3 \cdot 5H_2O$, $Gd(NO_3)_3 \cdot 5H_2O$, $Nd(NO_3)_3 \cdot 6H_2O$, and $Sm(NO_3)_3 \cdot 5H_2O$ as the precursors. In the molar ratio $Ti(OBu)_4 : C_2H_5OH : H_2O : HNO_3 = 1 : 20 : 6 : 0.8$, 12.5 ml $Ti(OBu)_4$ (C.P.) was dissolved in 33.3 ml ethanol with stirring for 10 min; then 0.25 ml HNO_3 was added dropwise

[1] To whom correspondence should be addressed. Fax: 86 20 84110318. E-mail: cedc17@zsu.edu.cn.

0021-9517/02 $35.00

to the above solution under stirring for 30 min. Another solution containing 16.7 ml ethanol, 1.5 ml H_2O, and rare earth metal salts in the required stoichiometry was slowly added into the above solution, the mixture was hydrolyzed at room temperature for 40 min under vigorous stirring, and the transparent sol was obtained. The gel was prepared by aging the sol for 48 h at room temperature. The derived gel was dried at 373 K for 24 h to remove the solvents and then fired in air at 773 K for 3 h and milled into powders for use. Pure TiO_2 was prepared in the same way.

2.2. Catalyst Characterization

Polycrystalline XRD patterns were obtained for the powdered samples using a Rigaku Max-3A. The diffraction patterns were recorded at room temperature using Ni-filtered Cu$K\alpha$ radiation ($\lambda = 0.15418$ nm) for all samples. The particle size was determined from the diffraction peak broadening with the Scherrer formula $D = 0.89\,\lambda/\beta \cos\theta$ (24). Unit cell volume was obtained by using Bragg's Law. The surface area of the samples was measured by N_2 adsorption at 77 K using the dynamic BET method using a Carlo Erba (Model 1800) sorptometer. The samples were outgassed in an evacuation chamber to a pressure of 10^{-3} atm at 393 K prior to adsorption. The IR analysis was carried out using KBr discs in the region of 4000–400 cm^{-1} by using FTIR-Bruker-EQUINOX-55 at ambient conditions. A Shimadzu spectrophotometer (Model 2501PC, Japan) equipped with an integrating sphere was used to record the diffuse reflectance spectra of the samples. The baseline correction was done using a calibrated sample of barium sulfate. The spectra were recorded at room temperature in air in the range of 300–900 nm. Samples used for the laser flash photolysis experiments were prepared by adding an aqueous suspension of the catalyst to a quartz cell (10 × 2 mm). The samples were excited with pulses from a Q-switch third-harmonic Nd:YAG laser (355 nm, 5 ns FWHM). Excitation pulse energies were ~10 mJ/pulse. Transient absorption kinetics was observed using a CW He-Ne laser as a probe. All decay kinetics was monitored by following the trapped charge carrier absorption at 544 nm. The measurements were performed under Ar bubbling. Three spectra for each sample were averaged to obtain the displayed spectra.

2.3. Photocatalytic Activity Testing

The photocatalytic activities of pure TiO_2 and RE/TiO_2 catalysts were tested by using nitrite degradation. Nitrite (NO_2^-) was chosen as a model compound because it is a representative inorganic pollutant in water. Experiments were performed in a Pyrex photochemical reactor with a 300-W high-pressure mercury lamp ($\lambda = 290$–450 nm, 365 nm peak intensity, GGZ-300Z, China). Running water was passed through the double wall to cool the reaction solution and remove the IR fraction of the beam. The photon flow per unit volume inside the cell, measured by uranyl oxalate actinometry, was 1.2×10^{-7} einsteins s^{-1} dm^{-3} and was kept constant in all experiments. All experimental conditions were kept constant as follows: catalyst concentration = 1 g dm^{-3}; initial nitrite concentration $C_0 = 1.2\ (\pm 0.1) \times 10^{-4}$ mol dm^{-3}; open, magnetic stirring; pH = 6.5. Before irradiation, suspensions were stirred for 30 min in the dark to ensure equilibration of nitrite over the oxide surface, and the amount of adsorption of nitrite on the oxides was tested. At least five photocatalytic experiments were carried out for each condition, averaging the results. No reaction was found in any case in the absence of the photocatalyst. After irradiation the solution was periodically withdrawn and centrifuged to remove almost all the catalyst, and the centrifugate was analyzed for nitrite. The concentration of nitrite was analyzed by standard *N*-(1-naphthyl) ethylene diamine hydrochloride colorimetric method. Absorbance was determined by 722 UV–vis spectrophotometer (Lingguang, China) at 540 nm. The error in the determinations was lower than 2.2%.

3. RESULTS

3.1. Catalyst Characterization

The XRD patterns showed that only anatase was found in all samples of rare-earth-doped TiO_2. Table 1 gives the characteristics of Sm^{3+}-doped samples containing different contents of Sm. Particle sizes of Sm^{3+}-doped samples slightly decrease with nominal content of Samarium increasing as compared with undoped TiO_2. The decrease in particle size can be attributed to the presence of Sm–O–Ti in the doped samples, which inhibits the growth of crystal grains (23). From the values given in Table 1 it is clear that there is not much change in unit cell volume between pure TiO_2 and Sm^{3+}-doped samples.

The results obtained from the diffuse reflectance spectra are shown in Fig. 1. The spectra of rare earth metal-doped TiO_2 show red shifts in the band gap transition. The absorption edge shifts to a longer wavelength in the order of $Gd^{3+} > Nd^{3+} > La^{3+} > Pr^{3+}$ $(Er^{3+}) > Ce^{3+} > Sm^{3+}$ doped samples (the DRS spectra of Nd^{3+}-, La^{3+}-, and

TABLE 1

Characteristics of Pure TiO_2 and Sm^{3+}-Doped TiO_2 with Different Doping Contents

Catalyst	Particle size (nm)	Surface area ($m^2\ g^{-1}$)	Unit cell volume (Å^3)
Pure TiO_2	20	35.7	136.51
0.1 wt%	17	38.9	136.46
0.5 wt%	13	44.5	136.55
1.0 wt%	14	40.6	136.64
2.0 wt%	16	37.3	136.49

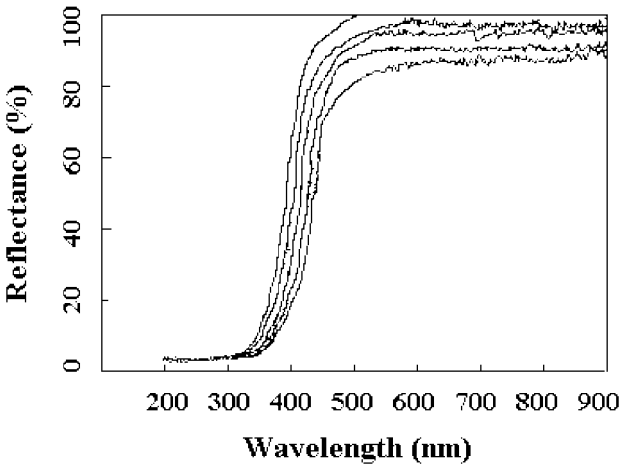

FIG. 1. Diffuse reflectance spectra of pure TiO_2 and Sm^{3+}-, Ce^{3+}-, Er^{3+}-, and Gd^{3+}-doped TiO_2 (from left to right, with the same content of 0.5 wt%).

Pr^{3+}-doped samples are not shown herein). Red shifts of this type can be attributed to the charge-transfer transition between the rare earth ion f electrons and the TiO_2 conduction or valence band (25). Moreover, the absorbance of the rare earth doped samples was found to increase with increasing in rare earth content.

3.2. FTIR Analysis

Infrared studies were used to identify the state of rare earth ions in the rare earth doped samples. By comparing IR spectra of Sm^{3+}-doped TiO_2 (3.0 wt% Sm dopping) and of pure TiO_2 (not shown herein), a new band at 490 cm^{-1} was observed in the spectra of Sm^{3+}-doped samples. This band is attributed to the Sm–O bond (26). It can be seen Sm ions dispersed on the surface of TiO_2 in the form of metal oxides. IR spectra also show other rare earth ions dispersed on TiO_2 particles in the form of rare earth oxides RE_2O_3 formed during the calcination process.

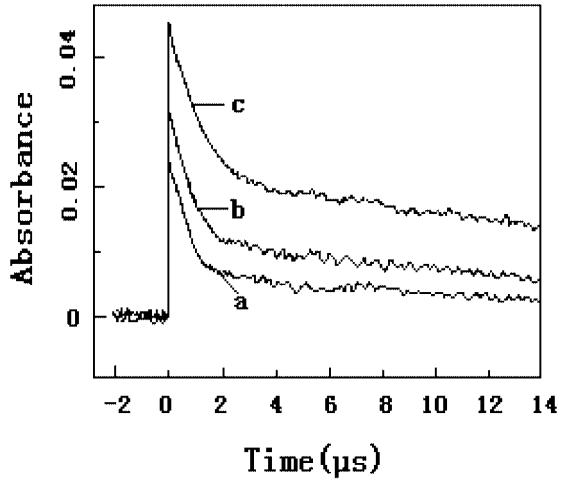

FIG. 2. Transient absorption decays observed at 544 nm in the microsecond time scale for (a) naked TiO_2; (b) Sm^{3+}-doped sample (0.5 wt%); (c) Gd^{3+}-doped sample (0.5 wt%).

TABLE 2

Comparison of the Fitting Parameters (Eq. [1]) from the Transient Absorption Decays with the Apparent Degradation Rate Constants

Dopant	A_∞ ($\times 10^{-3}$)	k_1 ($\times 10^7$)	k_2 ($\times 10^6$)	Apparent rate constant (mol dm^{-3} min^{-1})
Undoped	1.29	1.85	1.47	0.8×10^{-6}
Gd^{3+}	9.87	1.34	0.96	9.1×10^{-6}
Sm^{3+}	3.45	2.73	1.12	2.2×10^{-6}

3.3. Transient Absorption Spectra

The decay profiles of photoexcited absorption are shown in Fig. 2. All excited state decays in microsecond time region were fitted to the following double-exponential equation:

$$A(t) = A_\infty + B_1 \exp(-k_1 t) + B_2 \exp(-k_2 t). \qquad [1]$$

The fitting parameters for three samples and their corresponding reaction rate constants are listed in Table 2. No correlation was observed between the decay constants (k_1 and k_2) and the photocatalytic activity. However, the A_∞, which is determined from the plateau region, seems to correlate between A_∞ and the photoreactivity. A_∞ represents the residual absorption by the trapped charge carriers that survive recombination over the nano- to microsecond time domain (9).

3.4. Adsorption Measurements

The equilibrium adsorption of nitrite was studied. Suspensions were stirred for 30 min in the dark to ensure equilibration of nitrite over the oxide surface, and the amount of adsorption of nitrite on the oxides was tested by comparing the concentration before and after stirring. The saturation amount of nitrite adsorbed on Sm^{3+}-doped TiO_2 containing different content of Sm and other rare-earth-ion-doped samples is given in Table 3 and Table 4

TABLE 3

Equilibrium Adsorption of Nitrite in the Dark over Sm^{3+}-Doped TiO_2 Catalysts

Catalyst	Percentage of nitrite adsorbed (%)
0.0 wt%	3.5
0.1 wt%	5.6
0.5 wt%	6.5
1.0 wt%	5.1
2.0 wt%	4.0

TABLE 4

Equilibrium Adsorption of Nitrite in the Dark over Different Rare-Earth-Doped TiO_2

Catalyst	Percentage of nitrite adsorbed (%)
Pure TiO_2	3.5
1.0 wt% Sm^{3+}	5.1
1.0 wt% Ce^{3+}	7.1
1.0 wt% Er^{3+}	9.2
1.0 wt% Pr^{3+}	9.3
1.0 wt% La^{3+}	11.7
1.0 wt% Nd^{3+}	12.8
1.0 wt% Gd^{3+}	18.4

respectively. Percentage of nitrite adsorption was evaluated from $(1 - C/C_0) \times 100$, where C and C_0 represented the equilibrium concentration and the initial concentration of nitrite, respectively. From Table 3, it is observed that the amount of nitrite adsorbed on 0.5 wt% Sm^{3+}-doped TiO_2 shows the highest value. From Table 4, it can be seen that the amount of nitrite adsorbed on all rare-earth-doped samples is more than that of pure TiO_2, and the adsorption on Gd^{3+}-doped sample shows the highest value among all rare-earth-doped samples.

3.5. Photocatalytic Activity Measurement

The photocatalytic oxidation of nitrite over Sm^{3+}-doped samples was evaluated and the results are shown in Fig. 3. It is clear from Fig. 3 that 0.5 wt% Sm^{3+}-doped TiO_2 showed the most activity among all samples. Moreover, it can be seen that plots of Sm^{3+}-doped samples are linear, indicating that the disappearance of NO_2^- obeys a zero-order equation, i.e., $C/C_0 = 1 - (K/C_0)t$, since the reaction rate constant is independent of NO_2^- concentration. Zero-order

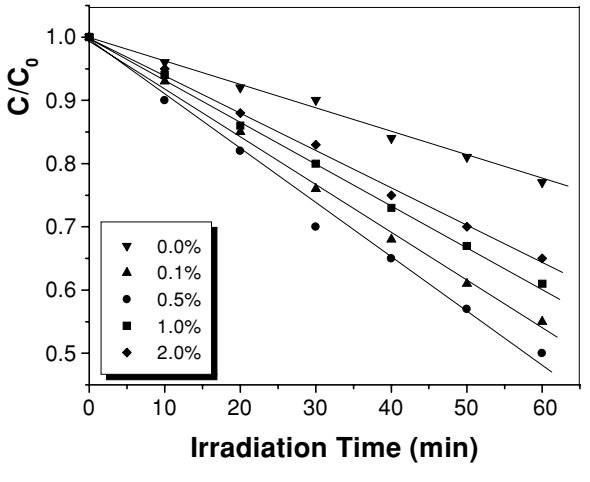

FIG. 3. Normalized concentration vs reaction time for nitrite degradation over Sm^{3+}-doped TiO_2 catalysts.

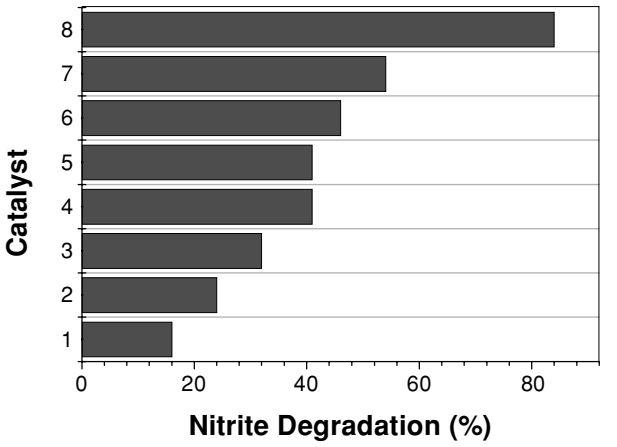

FIG. 4. Photocatalytic degradation conversion of nitrite over different rare earth doped TiO_2 catalysts. Catalyst: 1: pure TiO_2; 2: Sm^{3+} doping; 3: Ce^{3+} doping; 4: Er^{3+} doping; 5: Pr^{3+} doping; 6: La^{3+} doping; 7: Nd^{3+} doping; 8: Gd^{3+} doping with the same concentration (1.0 wt%).

kinetics was also observed for Ce^{3+}-, Er^{3+}-, Pr^{3+}-, La^{3+}-, and Nd^{3+}-doped TiO_2 catalysts in the degradation of nitrite. As we will discuss later, this behaviour could be explained on the basis of a high electron–hole recombination rate.

Figure 4 showed the results of the photocatalytic degradation of nitrite over the different rare earth doped samples with the same doping content (1.0 wt%) for 40 min irradiation. It is obvious that all rare earth doped samples shows higher reactivity than of pure TiO_2, and Gd^{3+}-doped TiO_2 sample exhibits the highest photocatalytic acvitity of all tested samples due to its particularity.

The photocatalytic degradation of nitrite over Gd^{3+}-doped TiO_2 catalysts and Degussa P-25 is given in Fig. 5. It is clear from Fig. 5 that 0.5 wt% Gd^{3+}-doped sample showed the highest activity among all samples at longer irradiation times. Although P-25 presented the highest initial rate together with the 0.5 wt% Gd^{3+}-doped sample, an inhibition corresponding ca. 75% NO_2^- conversion occurred after 20 min irradiation when using P-25, this result is

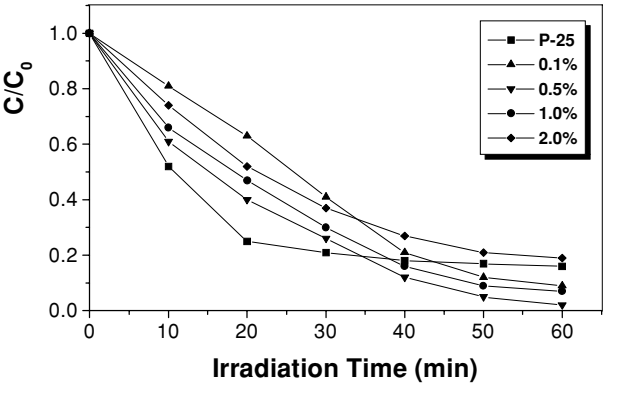

FIG. 5. Normalized concentration vs reaction time for nitrite degradation over Gd^{3+}-doped TiO_2 catalysts and Degussa P-25.

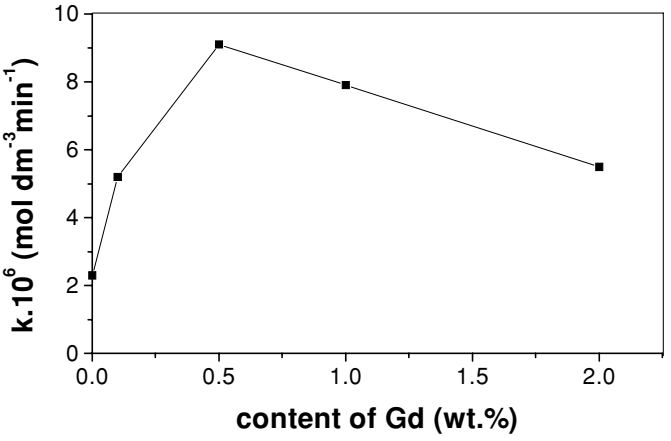

FIG. 6. Dependence of the rate constants on the content of Gd^{3+} in the TiO_2.

agreement with that of Hori *et al.* (27). Any inhibition was not found with the Gd^{3+}-doped samples. It can also be seen that the photocatalytic oxidation reactions of nitrite over Gd^{3+}-doped samples and P-25 follow the apparent first-order kinetics by analyzing this data. Figure 6 shows the rate constants k of nitrite oxidation over different content Gd^{3+}-doped samples, which were obtained by correlating the Langmuir–Hinshelwood kinetics model with these data (L–H relationship : $R = kKC/(1 + KC)$, where R is the reaction rate, k is the rate constant, and K is the adsorption equilibrium constant). It can be seen from Fig. 6 that the rate constant of the sample doped with 0.5 wt% Gd has the highest value (9.1×10^{-6} mol dm^{-3} min^{-1}).

4. DISCUSSION

The ionic radii of Sm^{3+}, Ce^{3+}, Er^{3+}, Pr^{3+}, La^{3+}, Nd^{3+}, and Gd^{3+} are 0.96, 1.03, 0.89, 1.01, 1.15, 0.99, and 0.94 Å, respectively (28), and much larger than that of Ti^{4+} (0.68 Å). Therefore, it is difficult for these rare earth ions to enter into the lattice of TiO_2. Unit cell volumes of RE-doped TiO_2 particles from XRD analysis (Table 1) are basically the same as that of undoped TiO_2, which obviously indicates that these rare earth ions cannot enter into the lattice of TiO_2 to replace the Ti^{4+} ion. IR spectra identify that rare earth salts were changed into rare earth oxides during the calcination process. These oxides were uniformly adsorbed on the surface of TiO_2 and may favor separating charge carriers efficiently, prolonging the life of carriers, inhibiting the recombination of electron–hole pairs, and eventually causing the enhancement of the reactivity. In addition, titanium atoms can substitute for rare earth ions in the lattice of rare earth oxides to form tetrahedral Ti sites because the ionic radius of Ti^{4+} is much smaller that those of rare earth ions. The Ti^{4+} ion replaces a rare earth ion with a +3 oxidation state and creates a charge imbalance. The charge imbalance must be satiated, so more hydroxide ions would be adsorbed onto the surface for charge balance. These hydroxide ions on the surface can accept holes generated by UV irradiation to form hydroxyl radicals, which oxidize adsorbed substrates. Therefore, the photoinduced charge carriers recombination can be suppressed.

DRS spectra of RE-doped catalysts show that the range of photoresponse increases and there exist red shifts in the doped samples, and the degree of red shift is different. As can be seen in Fig. 1, a little red shift of Sm^{3+}-doped sample and the largest red shift of Gd^{3+}-doped sample were observed. A closer inspection clarifies that the absorption edge shifts to a longer wavelength in the order of the samples doped with Gd^{3+}>Nd^{3+}>La^{3+}>Pr^{3+} (Er^{3+})>Ce^{3+}>Sm^{3+}, which is consistent with that of the photocatalytic activity. A larger red shift might indicate that the sample absorbs more photons and photoactivity is thus enhanced. Wang *et al.* (29) reported that the IPCEs (the incident monochromatic photon to current conversion efficiency) of Eu^{3+}-, La^{3+}-, Nd^{3+}-, and Pr^{3+}-doped TiO_2 electrodes were much larger than that of undoped TiO_2, and the IPCE of the Sm^{3+}-doped TiO_2 electrode was a little larger than that of the undoped TiO_2 electrode, which indicates that the photogenerated electron–hole pairs were separated more efficiently in rare-earth-doped TiO_2 nanoparticles than in pure TiO_2. A little higher activity of Sm^{3+}-doped sample is due to a little larger IPCE as compared to other RE-doped TiO_2. Our results are consistent with that of the IPCEs measured by Wang.

It is well known that the photocatalytic reaction occurs on the surface of the catalysts, and recombination of the photogenerated electron and hole is very fast (nanosecond timescale) (30, 31), so interfacial charge carrier transfer is possible only when the donor or acceptor is pre-adsorbed before the photocatalytic reaction. The preliminary adsorption of the substrates and the amount of adsorption are very important pre-requisites for highly efficient degradation. The results of adsorption measurements (Table 4) showed that the amount of Sm^{3+}-doped sample is the smallest, and that of Gd^{3+}-doped sample is the largest. In order of decreasing adsorption capacity they are Gd^{3+}->Nd^{3+}->La^{3+}->Pr^{3+}-(Er^{3+}-)>Ce^{3+}->Sm^{3+}-doped catalysts. All doping samples show the stronger adsorption capacities than pure TiO_2. The more amount of nitrite is adsorbed, the higher reactivity of the catalyst shows. The photocatalytic activity is positive correlation to the amount of adsorption over the catalysts (Table 3 and Fig. 3, Table 4 and Fig. 4). The results indicate that the amount of substrate adsorbed on the catalyst is an important factor affecting the photocatalytic activity.

The optimum concentration of rare earth doping at ca. 0.5 wt% may be due to the fact that there exists an optimum doping content of rare earth ions in TiO_2 particles for the most efficient separation of photoinduced electron–hole pairs. Pleskov (32) reported that the value of the

space charge region potential for the efficient separation of electron–hole pairs must be not lower than 0.2 V. As the concentration of dopant ions increases, the surface barrier becomes higher, and the space charge region becomes narrower, the electron–hole pairs within the region are efficiently separated by the large electric field before recombination. On the other hand, when the concentration of doping ions is high, the space charge region becomes very narrow and the penetration depth of light into TiO_2 greatly exceeds the space charge layer; therefore the recombination of the photogenerated electron–hole pairs in semiconductor become easier. Consequently, there is an optimum concentration of dopant ions to make the thickness of space charge layer substantially equal to the light penetration depth. But for small colloidal particles, there is nearly no band-bending and the electrical field in colloidal semiconductors is usually small, so high dopant levels are favorable in producing a significant potential difference (permanent electric field) between the surface and the center of the particles to separate photoinduced electron–hole pairs efficiently (33). Moreover, the band-gap energies of the rare earth oxides used in the experiments are not sufficient for initiating photocatalytic reaction after UV irradiation (34). Excess amounts of rare earth oxide covering the surface of TiO_2 would increase the number of recombination centers and result in low photoactivity. So it is not a surprise that the mixed TiO_2-rare earth oxides with more than 0.5 wt% rare earth show poor photocatalytic activity. At the same time, the Sm^{3+}-doped sample at 0.5 wt% shows the most adsorption amount of nitrite, this could be another reason causing the activity of the sample with 0.5 wt% doping to be the highest.

The Gd^{3+}-doped sample has the highest reactivity among all concerned rare earth doped samples (as shown in Fig. 4). The main reason may be that gadolinium is a special element in rare earth elements. The Gd^{3+} has 7 f-electrons and is half filled, which is different from the other rare earth ions. Choi *et al.* (9) presented the results of a systematic study of the effects of 21 different metal ion dopants on the photochemical reactivity of quantum-sized TiO_2 with respect to both chloroform oxidation and carbon tetrachloride reduction. The largest enhanced photoactivity was seen for Fe^{3+}-, Ru^{3+}-, and Os^{3+}-doped samples. These three metal ions have the half-filled electronic configuration. Some general trends are apparent based on considerations of the electronic configuration of the dopants. It is well known that half-filled electronic configuration is of more stability. When Gd^{3+} ions trap electrons, the half-filled electronic configuration is destroyed and their stability decreases, the trapped electrons can easily be transferred to the oxygen molecules adsorbed on the surface of the catalysts, and the Gd^{3+} ions return to the original stable half-filled electronic structure. This might promote charge transfer and efficiently separate the electrons and holes by shallowly trapping electrons. The prerequisite for an effective dopant may involve the possibility of charge detrapping and migration to the surface of catalysts. Other rare earth ions might deeply trap the photoexcited electrons which are difficult to detrap and migrate to the surface of previouly trapped charges. So Gd^{3+}-doped TiO_2 has higher efficiency in the separation and transfer of charge carriers and shows higher reactivity than other rare-earth-doped samples. This is a possible mechanistic role of Gd^{3+} ions with half-filled f-shells in enhancing photocatalytic activity. DRS spectra (Fig. 1) indicated that the Gd^{3+}-doped sample has the biggest red shift and absorbance. The largest amount of adsorption, the half-filled electronic configuration, and the largest red shift of the Gd^{3+}-doped samples would contribute to its highest enhancement photoreactivity in the degradation of nitrite. The result is in good agreement with transient absorption measurements (Fig. 2). In general, a relative increase in the interfacial electron transfer rate results in a corresponding increase in photoreactivity. The photocatalytic degradation reaction of nitrite over Gd^{3+}-doped sample and P-25 follows Langmuir–Hinshelwood kinetics (Fig. 5), which are different from those of Sm^{3+}-, Ce^{3+}-, Er^{3+}-, Pr^{3+}-, La^{3+}-, and Nd^{3+}-doped TiO_2 catalysts, which obey zero-order kinetics (Fig. 3). Zero-order kinetic behavior could be explained on the basis of a high electron–hole recombination rate.

During the photocatalytic process, the absorption of photons by the photocatalyst leads to the excitation of electrons from the valence band to the conduction band, thus generating electron–hole pairs. The electron in the conduction band is captured by oxygen molecules dissolved in the suspension, and the hole in the valence band can be captured by OH^- or H_2O species adsorbed on the surface of the catalysts, to produce the hydroxyl radical. It has been assumed that NO_2^- is oxidized by hydroxyl radicals:

$$h^+ + OH^- \rightarrow {}^{\cdot}OH \qquad [2]$$

$$h^+ + H_2O \rightarrow {}^{\cdot}OH + H^+ \qquad [3]$$

$$NO_2^- + 2\,{}^{\cdot}OH \rightarrow NO_3^- + H_2O. \qquad [4]$$

The presence of zero-order kinetics indicated that the availability of holes on the surface was the rate determining step. In fact, considering the concentration of NO_2^- ions to be in excess in respect to trapped holes, and due to the fact that the number of holes only depend on the intensity of incident light, which was kept constant along the experiments, the above mechanism can explain the zero-order kinetics. The shortage of trapped holes which, on the other hand, does not take place in the samples of Gd^{3+} doping, may be explained by considering that interfacial electron transfer rate increases when Gd^{3+} is present in the TiO_2 matrix as discussed above.

5. CONCLUSION

In conclusion, doping rare earth ions in TiO_2 to form mixed RE/TiO_2 catalysts can enhance photocatalytic activity in the degradation of nitrite. The increase in activity is probably due to the higher adsorption, red shifts, and prevention of electron–hole recombination. The highest enhancement in photoreactivity was obtained at ca. 0.5 wt% rare-earth-ion doping, which may be in favor of the most efficient separation of the charge carriers. Gd^{3+}-doped TiO_2 shows the highest activity among all rare-earth-doped samples investigated because of the increase in the interfacial electron transfer rate. The activity differences are due to the change in the amount of surface hydroxyl groups resulting from the interaction between the rare earth oxides and titania. The photocatalytic degradation reaction of nitrite over Gd^{3+}-doped sample and P-25 follows the apparent first order kinetics, which is different from that of Sm^{3+}-, Ce^{3+}-, Er^{3+}-, Pr^{3+}-, La^{3+}-, and Nd^{3+}-doped TiO_2 catalysts, which obey zero-order kinetics, indicating that the photochemical process is dominated by electron–hole recombination.

REFERENCES

1. Hoffmann, M. R., Martin, S. T., Choi, W., and Bahnemann, D. W., *Chem. Rev.* **95**, 69 (1995).
2. An-Wu Xu, Han-Qin Liu, and Yu-Guang Li, *Chem. J. Chin. Univ.* **8**, 1252 (2000).
3. Peral, J., and Ollis, D. F., *J. Catal.* **136**, 554 (1992).
4. Zorn, M. E., Tompkins, D. T., and Zeltner, W. A., *Appl. Catal. B-Environ.* **1**, 1 (1999).
5. Brezova, V., and Stasko, A. J., *J. Catal.* **147**, 156 (1994).
6. Ollis, D. F., and Al-Ekabli, H., "Photocatalytic Purification and Treatment of Water and Air." Elsevier, Amsterdam, 1993.
7. Rekoske, J. E., and Barteau, M., *J. Catal.* **165**, 57 (1997).
8. Ranjit, K. T., and Viswanathan, B., *J. Photochem. Photobiol. A Chem.* **107**, 215 (1997).
9. Choi, W., Termin, A., and Hoffmann, M. R., *J. Phy. Chem.* **98**, 13669 (1994).
10. Litter, M. I., and Navio, J. A., *J. Photochem. Photobiol. A Chem.* **98**, 171 (1996).
11. Palmisano, L., Auguliaro, V., Sclafani, A., and Schiavello, M., *J. Phys. Chem.* **92**, 6710 (1988).
12. Martin, C., Martin, I., Rives, V., Paimisano, L., and Schiavello, M., *J. Catal.* **134**, 434 (1992).
13. Soria, J., Conesa, J. C., and Augugliaro, V., *et al., J. Phys. Chem.* **95**, 274 (1991).
14. Luo, Z., and Gao, Q. H., *J. Photochem. Photobiol. A Chem.* **63**, 367 (1992).
15. Takeda, N., Iwata, N., Torimoto, T., and Yoneyama, H., *J. Catal.* **177**, 240 (1998).
16. Sampath, S., Uchida, H., and Yoneyama, H., *J. Catal.* **149**, 189 (1994).
17. Nobile, Jr., A., and Davis, M. W., *J. Catal.* **116**, 383 (1989).
18. Romero, M., Blanco, J., and Sanchez, B., *et al., Solar Energy* **2**, 169 (1999).
19. Moser, J., Punchihewa, S., Infelta, P. P., and Gratzel, M., *Langmuir* **7**, 3012 (1991).
20. Hong, A. P., Bahnemann, D. W., and Hoffmann, M. R., *J. Phys. Chem.* **91**, 2109 (1987).
21. Lin, J., Yu, J. C., Lo, D., and Lam, S. K., *J. Catal.* **183**, 368 (1999).
22. Serpone, N., and Lawless, D., *Langmuir* **10**, 643 (1994).
23. Lin, J., and Yu, J. C., *J. Photochem. Photobiol. A Chem.* **116**, 63 (1998).
24. Klug, H. P., and Alexander, L. E., "X-ray Diffraction Procedures." Wiley, New York, 1967.
25. Borgarello, E., Kiwi, J., Gratzel, M., Pelizzetti, E., and Visca, M., *J. Am. Chem. Soc.* **104**, 2996 (1982).
26. Yang, Y. P., and Huang, K. L., *J. Rare Earth* **4**, 20 (1996). [In Chinese]
27. Hori, Y., Bandoh, A., and Nakatsu, A., *J. Electrochem. Soc.* **137**, 1155 (1990).
28. Evans, R. C., "An Introduction to Crystal Chemistry," 2nd ed., p. 38. Cambridge Univ. Press, Cambridge, UK, 1964.
29. Wang, Y. Q., Cheng, H. M., Zhang, L., Hao, Y. Z., Ma, J. M., Xu, B., and Li, W. H., *J. Mol. Catal. A Chem.* **151**, 205 (2000).
30. Colombo, Jr., D. P., and Bowman, R. M., *J. Phys. Chem.* **99**, 11752 (1995).
31. Rothenberger, G., Moser, J., Gratzel, M., Serpone, N., and Sharma, D. K., *J. Am. Chem. Soc.* **107**, 8054 (1985).
32. Pleskov, Y. V., *Sov. Electrochem.* **17**, 1 (1981).
33. Hagfeldt, A., and Gratzel, M., *Chem. Rev.* **95**, 49 (1995).
34. Gschneidner, K. A., Eyring, Jr., L., Choppin, G. R., and Lander, G. H., "Handbook on the Physics and Chemistry of Rare Earths," p. 448. North-Holland, Amsterdam, 1994.